

## Diffraction at HERA: experimental perspective

Anthony T Doyle

### Abstract

Measurements of diffractive phenomena observed at HERA are reviewed. A short introduction to the theoretical background is presented. The review focuses on the current experimental directions and discusses the exclusive production of vector mesons, the deep inelastic structure of diffraction and complementary information from jet structures. Emphasis is placed on the current sources of background and the experimental uncertainties.

*Talk presented at the Workshop on HERA Physics,  
“Proton, Photon and Pomeron Structure”,  
Durham, September 1995.*

# 1 Introduction: maps of the pomeron

At the last Durham workshop on HERA physics, HERA was heralded as the new frontier for QCD. In the proceedings from that workshop, there was one theoretical contribution on “Partons and QCD effects in the pomeron” [1]. Experimentally, the large rapidity gap events in deep inelastic scattering were yet to be discovered and the first preliminary results on photoproduced vector mesons were just starting to appear. Two years later, this workshop focuses on “proton, photon and pomeron structure”: the inclusion of the word “pomeron” in the title of the workshop reflects a series of diffractive measurements which have been made in the intervening period at HERA. This talk is therefore an opportunity to discuss “*Measurements of partons and QCD effects in the pomeron*”, based on results from the H1 and ZEUS collaborations.

The diffractive processes studied are of the form:

$$e(k) + p(P) \rightarrow e'(k') + p'(P') + X,$$

where the photon dissociates into the system  $X$  and the outgoing proton,  $p'$ , remains intact, corresponding to single dissociation. The measurements are made as a function of the photon virtuality,  $Q^2 \equiv -q^2 = -(k - k')^2$ , the centre-of-mass energy of the virtual-photon proton system,  $W^2 = (q + P)^2$ , the mass of the dissociated system,  $X$ , denoted by  $M^2$  and the four-momentum transfer at the proton vertex, given by  $t = (P - P')^2$ .

The subject of diffraction is far from new: diffractive processes have been measured and studied for more than thirty years [2]. Their relation to the corresponding total cross sections at high energies has been successfully interpreted via the introduction of a single pomeron trajectory with a characteristic  $W^2$  and  $t$  dependence [3]. The high-energy behaviour of the total cross sections is described by a power-law dependence on  $W^2$ :

$$\sigma \sim (W^2)^\epsilon \tag{1}$$

where  $W$  is measured in GeV,  $\epsilon = \alpha(0) - 1$  and  $\alpha(0)$  is the pomeron intercept. The slow rise of hadron-hadron total cross sections with increasing energy indicates that the value of  $\epsilon \simeq 0.08$  i.e. the total cross sections increase as  $W^{0.16}$ , although the latest  $p\bar{p}$  data from CDF at  $\sqrt{s} = 1800$  GeV indicate  $\epsilon \simeq 0.11$  [4]. The optical theorem relates the total cross sections to the elastic, and hence diffractive, scattering amplitude at the same  $W^2$ :

$$\frac{d\sigma}{dt} \sim (W^2)^{2(\epsilon - \alpha' \cdot |t|)} \tag{2}$$

where  $\epsilon - \alpha' \cdot |t| = \alpha(t) - 1$  and  $\alpha' = 0.25 \text{ GeV}^{-2}$  reflects the shrinkage of the diffractive peak with increasing  $W^2$ .

Whilst these Regge-based models give a unified description of all pre-HERA diffractive data, this approach is not fundamentally linked to the underlying theory of QCD. It has been anticipated that at HERA energies if either of the scales  $Q^2$ ,  $M^2$  or  $t$  become larger than the QCD scale  $\Lambda^2$ , then it may be possible to apply perturbative QCD (pQCD) techniques, which predict changes to this power law behaviour, corresponding to an increase in the effective value of  $\epsilon$  and a decrease of  $\alpha'$ . This brings us from the regime of dominance of the slowly-rising “soft” pomeron to the newly emergent “hard” behaviour and the question of how a transition may occur between the two. Precisely where the Regge-based approach breaks down or where

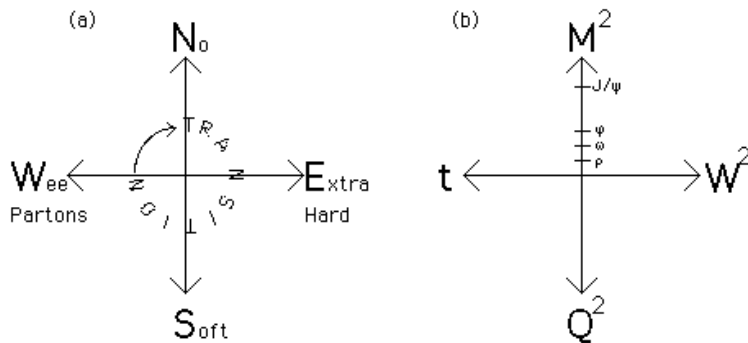


Figure 1: Maps of the pomeron: (a) theoretical and (b) experimental directions.

pQCD may be applicable is open to experimental question. The emphasis is therefore on the internal (in)consistency of a wide range of measurements of diffractive and total cross sections. As an experimentalist navigating around the various theoretical concepts of the pomeron, it is sometimes difficult to see which direction to take and what transitions occur where (Figure 1(a)). However, from an experimental perspective, the directions are clear, even if the map is far from complete (Figure 1(b)).

The HERA collider allows us to observe a broad range of diffractive phenomena at the highest values of  $W^2$ . What is new is that we have the ability to observe the variation of these cross sections at specific points on the  $M^2$  scale, from the  $\rho^0$  up to the  $\Upsilon$  system as discussed in section 2.1. Similarly, the production cross section can be explored as a function of  $Q^2$ , using a virtual photon probe. The high energy available provides a large rapidity span of  $\simeq 10$  units ( $\Delta(\eta) \sim \ln(W^2)$ ). The observation of a significant fraction of events ( $\simeq 10\%$ ) with a large rapidity gap between the outgoing proton,  $p'$ , and the rest of the final state,  $X$ , in deep inelastic scattering (DIS) has led to measurements of the internal structure of the pomeron. These results are discussed in section 2.2. Similar studies of events with high- $p_T$  jets and a large rapidity gap have also been used to provide complementary information on this structure. Also, the observation of rapidity gaps between jets, corresponding to large  $t$  diffraction, are presented in section 2.3. Finally, a first analysis of the leading proton spectrometer data where the diffracted proton is directly measured is presented in section 2.4.

## 2 Signals and Backgrounds

### 2.1 Exclusive Production of Vector Mesons

The experimental signals are the exclusive production of the vector mesons in the following decay modes:

$$\rho^0 \rightarrow \pi^+\pi^- [5, 6, 7, 8] \quad \phi \rightarrow K^+K^- [9, 10] \quad J/\psi \rightarrow \mu^+\mu^-, e^+e^- [11, 12, 13].$$

First results on  $\omega \rightarrow \pi^+\pi^-\pi^0$  and higher vector mesons ( $\rho' \rightarrow \pi^+\pi^-\pi^0\pi^0$  and  $\psi' \rightarrow \mu^+\mu^-, e^+e^-$ ) are in the early analysis stages and first candidates for  $\Upsilon \rightarrow \mu^+\mu^-, e^+e^-$  are also appearing in the data.

The clean topology of these events results in typical errors on the measured quantities ( $t$ ,  $M^2$ ,  $W^2$  and  $Q^2$ ), reconstructed in the tracking chambers, of order 5%. Containment within the tracking chambers corresponds to a  $W$  interval in the range  $40 \lesssim W \lesssim 140$  GeV. However, some analyses are restricted to a reduced range of  $W$  where the tracking and trigger systematics are well understood. Conversely, H1 have also used the shifted vertex data to extend the analysis of the  $\rho^0$  cross section to higher  $\langle W \rangle = 187$  GeV. At small  $t$  there are problems triggering and, to a lesser extent, reconstructing the decay products of the vector meson. In particular, the photoproduction of  $\phi$  mesons is limited to  $t \gtrsim 0.1$  GeV<sup>2</sup>, since the produced kaons are just above threshold and the available energy in the decay is limited. In order to characterise the  $t$ -dependence, a fit to the diffractive peak is performed. In the most straightforward approach, a single exponential fit to the  $t$  distribution,  $dN/d|t| \propto e^{-b|t|}$  for  $|t| \lesssim 0.5$  GeV<sup>2</sup> is adopted.

The contributions to the systematic uncertainties are similar in each of the measurements. For example, the uncertainties on acceptance of photoproduced  $\rho^0$ 's are due to uncertainties on trigger thresholds ( $\simeq 9\%$ ), variations of the input Monte Carlo distributions ( $\simeq 9\%$ ) and track reconstruction uncertainties especially at low  $p_T$  ( $\simeq 6\%$ ). In particular for the  $\rho^0$  analysis, where the mass distribution is skewed compared to a Breit-Wigner shape, uncertainties arise due to the assumptions of the fit for the interference between the resonant signal and the non-resonant background contributions ( $\simeq 7\%$ ). Other significant contributions to the uncertainty are contamination due to  $e$ -gas interactions ( $\simeq 2$ -5%) and from higher mass dissociated photon states, such as elastic  $\omega$  and  $\phi$  decays ( $\simeq 2$ -7%). The uncertainty due to neglecting radiative corrections can also be estimated to be  $\simeq 4$ -5% [5, 6].

Finally, one of the key problems in obtaining accurate measurements of the exclusive cross sections and the  $t$  slopes is the uncertainty on the double dissociation component, where the proton has also dissociated into a low mass nucleon system [14]. The forward calorimeters will see the dissociation products of the proton if the invariant mass of the nucleon system,  $M_N$ , is above approximately 4 GeV. A significant fraction of double dissociation events produce a limited mass system which is therefore not detected. Proton remnant taggers are now being used further down the proton beamline to provide constraints on this fraction and, in the H1 experiment, further constraints are provided by measuring secondary interactions in the forward muon system. Based on  $p\bar{p}$  data one finds that the dissociated mass spectrum falls as  $dN/dM_N^2 = 1/M_N^n$  with  $n = 2.20 \pm 0.03$  at  $\sqrt{s} = 1800$  GeV from CDF measurements [15]. However it should be noted that this measurement corresponds to a restricted mass interval. The extrapolation to lower masses is subject to uncertainties and the universality of this dissociation is open to experimental question, given the different behaviour at the upper vertex. Precisely how the proton dissociates and whether the proton can be regarded as dissociating independently of the photon system is not a priori known. Currently, this uncertainty is reflected in the cross sections by allowing the value of  $n$  to vary from around 2 to 3, although this choice is somewhat arbitrary. The magnitude of the total double dissociation contribution is estimated to be typically  $\simeq 50\%$  prior to cuts on forward energy deposition, a value which can be cross-checked in the data with an overall uncertainty of  $\simeq 10\%$  which is due to the considerations above. Combining the above uncertainties, the overall systematic errors in the various cross sections are typically  $\simeq 20\%$ .

Photoproduction processes have been extensively studied in fixed-target experiments, providing a large range in  $W$  over which to study the cross sections. The key features are the weak dependence of the cross section on  $W$ , an exponential dependence on  $t$  with a slope which

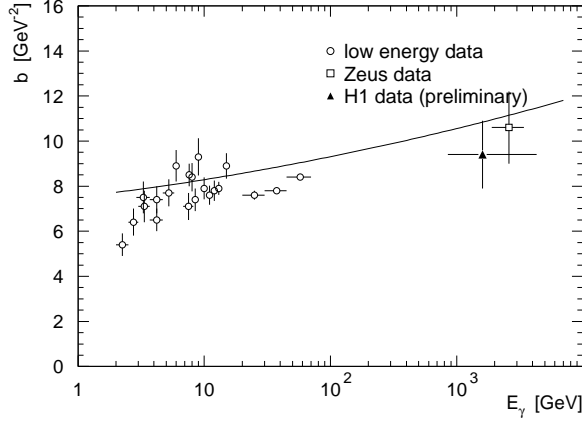


Figure 2: Dependence of the exponential slope parameter  $b$  as a function of  $E_\gamma$  for exclusive  $\rho^0$  photoproduction compared to the soft pomeron exchange prediction of Schuler and Sjöstrand.

shrinks with increasing  $W$  and the retention of the helicity of the photon by the vector meson. The  $t$  dependence of the  $\rho^0$  photoproduction data is illustrated in Figure 2 where the H1 and ZEUS data are compared to a compilation of lower energy data [16]. The data are consistent with a shrinkage of the  $t$  slope with increasing  $E_\gamma \simeq W^2/2$ , where  $E_\gamma$  is the photon energy in the proton rest frame, as indicated by the curve for soft pomeron exchange [17].

The measured  $t$  slopes are  $9.4 \pm 1.4 \pm 0.7 \text{ GeV}^{-2}$  (H1) [5] and  $10.4 \pm 0.6 \pm 1.1 \text{ GeV}^{-2}$  (ZEUS) [6] for the  $\rho^0$  (where similar single-exponential fits have been applied). These values can be compared to  $7.3 \pm 1.0 \pm 0.8 \text{ GeV}^{-2}$  (ZEUS) [9] for the  $\phi$  and  $4.7 \pm 1.9 \text{ GeV}^{-2}$  (H1) [11] for the  $J/\psi$ . Physically, the slope of the  $t$  dependence in diffractive interactions tells us about the effective radius of that interaction,  $R$ : if  $d\sigma/dt \propto e^{-b|t|}$ , then  $b \simeq 1/4 R^2$ . The range of measured  $b$  slopes varies from around  $4 \text{ GeV}^{-2}$  ( $R \simeq 0.8 \text{ fm}$ ) to  $10 \text{ GeV}^{-2}$  ( $R \simeq 1.3 \text{ fm}$ ). Further, the interaction radius can be approximately related to the radii of the interacting proton and vector meson,  $R \simeq \sqrt{R_P^2 + R_V^2}$ . Given  $R_P \simeq 0.7 \text{ fm}$ , then this variation in  $b$  slopes corresponds to a significant change in the effective radius of the interacting vector meson from  $R_V \simeq 0.4 \text{ fm}$  to  $R_V \simeq 1.1 \text{ fm}$ .

Integrating over the measured  $t$  dependence, the  $W$  dependence of the results on exclusive vector meson photoproduction cross sections are shown in Figure 3 [18]. From the experimental perspective, there is generally good agreement on the measured cross sections. The  $\gamma p$  total cross section is also shown in Figure 3, rising with increasing energy as in hadron-hadron collisions and consistent with a value of  $\epsilon \simeq 0.08$  i.e. the total cross section increases as  $W^{0.16}$ .

Given the dominance of the pomeron trajectory at high  $W$  and an approximately exponential behaviour of the  $|t|$  distribution with slope  $b \simeq 10$ , whose mean  $|\bar{t}|$  value is given by  $1/b$ , the diffractive cross section rise is moderated from

$$W^{4\epsilon} = W^{0.32}$$

to

$$W^{4(\epsilon - \alpha'|\bar{t}|)} \equiv W^{4\bar{\epsilon}} = W^{0.22}.$$

Here  $\bar{\epsilon} = 0.055$  characterises the effective energy dependence after integration over  $t$ . The observed shrinkage of the diffractive peak therefore corresponds to a relative reduction of the

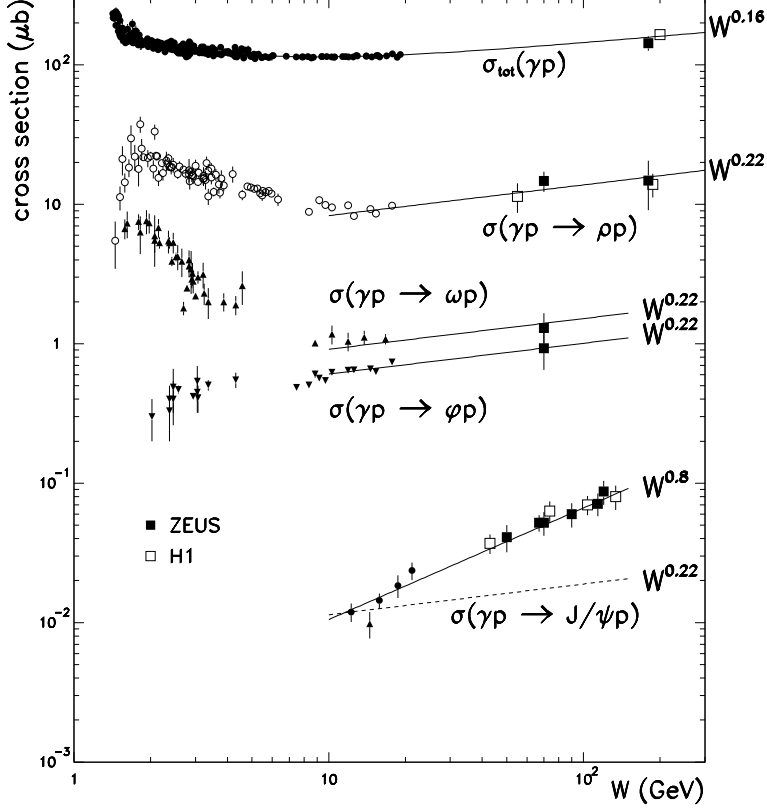


Figure 3:  $W$  dependence of the exclusive vector meson and total photoproduction cross sections compared to various power law dependences discussed in the text.

diffractive cross section with increasing energy. Such a dependence describes the general increase of the  $\rho^0$ ,  $\omega$  and  $\phi$  vector meson cross sections with increasing  $W$ . However, the rise of the  $J/\psi$  cross section is clearly not described by such a  $W$  dependence, the increase being described by an effective  $W^{0.8}$  dependence. Whilst these effective powers are for illustrative purposes only, it is clear that in exclusive  $J/\psi$  production a new phenomenon is occurring.

Qualitatively, the  $W^{0.8}$  dependence, corresponding to  $\bar{\epsilon} \simeq 0.2$ , could be ascribed to the rise of the gluon density observed in the scaling violations of  $F_2$ . The  $J/\psi$  mass scale,  $M^2$ , is larger than the QCD scale  $\Lambda^2$ , and it is therefore possible to apply pQCD techniques. Quantitatively, the theoretical analysis predicts that the rise of the cross section is proportional to the square of the gluon density at small- $x$  and allows discrimination among the latest parametrisations of the proton structure function [19]. We also know from measurements of the DIS  $\gamma^*p$  total cross section that application of formula (1) results in a value of  $\epsilon$  which increases with increasing  $Q^2$ , with  $\epsilon \simeq 0.2$  to  $0.25$  at  $Q^2 \simeq 10 \text{ GeV}^2$  [18]. The fact that the corresponding relative rise of  $F_2$  with decreasing  $x$  can be described by pQCD evolution [20] points towards a calculable function  $\epsilon = \epsilon(Q^2)$  for  $Q^2 \gtrsim Q_0^2 \simeq 0.3 \text{ GeV}^2$ .

One contribution to the DIS  $\gamma^*p$  total cross section is the electroproduction of low mass vector mesons. Experimentally, the statistical errors typically dominate with systematic uncertainties similar to the photoproduction case. The trigger uncertainties are significantly reduced, however, since the scattered electron is easily identified and the radiative corrections, which are more significant ( $\simeq 15\%$  [21]), can be corrected for. The  $W$  dependence of the DIS  $\rho^0$  and

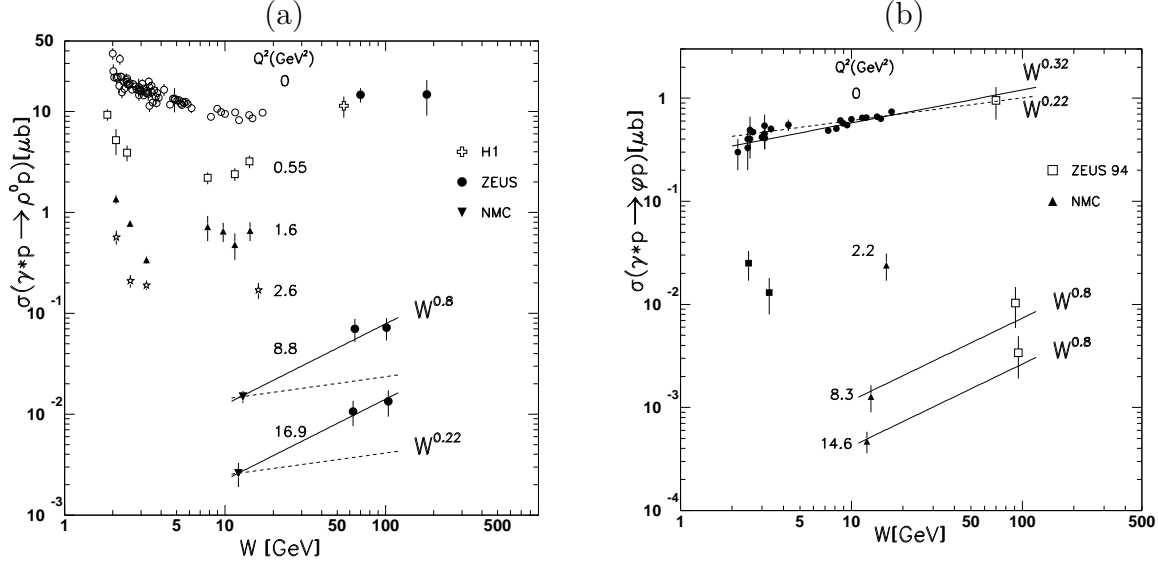


Figure 4:  $W$  dependence of exclusive (a)  $\rho^0$  and (b)  $\phi$  electroproduction cross sections for fixed values of  $Q^2$  compared to various power law dependences discussed in the text.

$\phi$  cross sections for finite values of  $Q^2$  are shown in Figure 4, compared to the corresponding photoproduction cross sections. The  $W$  dependence for the  $\rho^0$  and  $\phi$  electroproduction data are similar to those for the  $J/\psi$  photoproduction data, consistent with an approximate  $W^{0.8}$  dependence also shown in Figure 4. An important point to emphasise here is that the relative production of  $\phi$  to  $\rho^0$  mesons approaches the quark model prediction of  $2/9$  at large  $W$  and large  $Q^2$ , which would indicate the applicability of pQCD to these cross sections. The measurements of the helicity angle of the vector meson decay provide a measurement of  $R = \sigma_L/\sigma_T$  for the (virtual) photon, assuming s-channel helicity conservation, i.e. that the vector meson preserves the helicity of the photon. The photoproduction measurements for the  $\rho^0$  are consistent with the interaction of dominantly transversely polarised photons ( $R = 0.06 \pm 0.03$  (ZEUS) [6]). However, adopting the same analysis for virtual photons,  $R = 1.5^{+2.8}_{-0.6}$  (ZEUS) [8], inconsistent with the behaviour in photoproduction and consistent with a predominantly longitudinal exchange. This predominance is expected for an underlying interaction of the virtual photon with the constituent quarks of the  $\rho^0$ . Also, the measured  $b$  slope approximately halves from the photoproduction case to a value of  $b = 5.1^{+1.2}_{-0.9} \pm 1.0$  (ZEUS) [8], comparable to that in the photoproduced  $J/\psi$  case. The basic interaction is probing smaller distances, which allows a first comparison of the observed cross section with the predictions of leading-log pQCD (see [8]).

Finally, first results based on the observation of 42  $J/\psi$  events at significant  $\langle Q^2 \rangle = 17.7$  GeV $^2$  have been reported by H1 [13]. The cross section has been evaluated in two  $W$  intervals in order to obtain an indication of the  $W$  dependence, as shown in Figure 5, where an estimated 50% contribution due to double dissociation has been subtracted [22]. The electroproduction data are shown with statistical errors only although the systematics are estimated to be smaller than these errors ( $\simeq 20\%$ ). The electroproduction and photoproduction  $J/\psi$  data are consistent with the  $W^{0.8}$  dependence ( $\bar{\epsilon} \simeq 0.2$ ) noted previously. The  $J/\psi$  electroproduction cross section is of the same order of that of the  $\rho^0$  data, in marked contrast to the significantly lower photoproduction cross section for the  $J/\psi$ , even at HERA energies, also

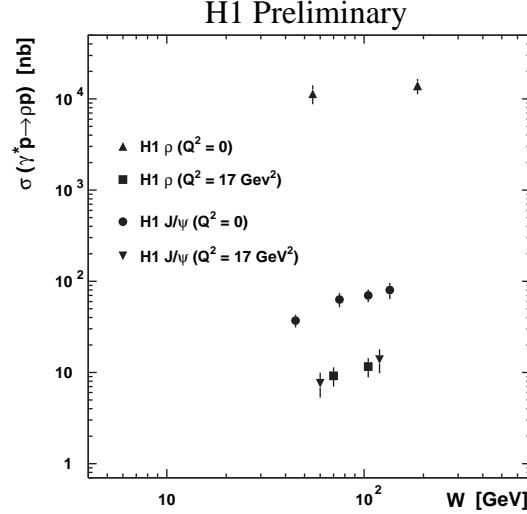


Figure 5: H1 measurements of the  $W$  dependence of electroproduction and photoproduction cross sections of exclusive vector mesons.

shown in Figure 5. Further results in this area would allow tests of the underlying dynamics for transverse and longitudinally polarised photons coupling to light and heavy quarks in the pQCD calculations.

In conclusion, there is an accumulating body of exclusive vector meson production data, measured with a systematic precision of  $\simeq 20\%$ , which exhibit two classes of  $W^2$  behaviour: a slow rise consistent with that of previously measured diffractive data for low  $M^2$  photoproduction data but a significant rise of these cross sections when a finite  $Q^2$  and/or a significant  $M^2$  is measured.

## 2.2 Deep Inelastic Structure of Diffraction

One of the major advances in the subject of diffraction has been the observation of large rapidity gap events in DIS and their subsequent analysis in terms of a diffractive structure function [23, 24]. In these analyses, the signature of diffraction is the rapidity gap, defined by measuring the maximum pseudorapidity of the most-forward going particle with energy above 400 MeV,  $\eta_{max}$ , and requiring this to be well away from the outgoing proton direction. A typical requirement of  $\eta_{max} < 1.5$  corresponds to a low mass state measured in the detectors of  $\ln(M^2) \sim 3$  units and a large gap of  $\ln(W^2) - \ln(M^2) \sim 7$  units with respect to the outgoing proton (nucleon system). In order to increase the lever arm in  $M^2$ , the H1 and ZEUS analyses have extended the  $\eta_{max}$  cuts to 3.2 and 2.5, respectively. This is achieved directly using the forward muon system/proton remnant taggers, in the case of H1, or via the measurement of a further discriminating variable,  $\cos\theta_H = \sum_i p_{z_i} / |\sum_i \vec{p}_i|$ , where  $\vec{p}_i$  is the momentum vector of a calorimeter cell, for ZEUS. These extensions are, however, at the expense of a significant non-diffractive DIS background (up to  $\simeq 50\%$  and  $\simeq 20\%$ , respectively). In each case, this background is estimated using the the colour-dipole model as implemented in the ARIADNE 4.03 program [26], which reasonably reproduces the observed forward  $E_T$  flows in non-diffractive interactions. The uncertainty on this background is estimated by changing



the applied cuts or by using other Monte Carlo models and is up to 20% for large masses,  $M^2$ , of the dissociated photon. The double dissociation contribution is estimated with similar uncertainties to the vector meson case. Other systematic errors are similar to those for the  $F_2$  analyses ( $\lesssim 10\%$ ) with additional acceptance uncertainties due to variations of the input diffractive Monte Carlo distributions.

In the presentation of the results, the formalism changes [25], reflecting an assumed underlying partonic description, and two orthogonal variables are determined:

$$x_P = \frac{(P - P') \cdot q}{P \cdot q} \simeq \frac{M^2 + Q^2}{W^2 + Q^2} \quad \beta = \frac{Q^2}{2(P - P') \cdot q} \simeq \frac{Q^2}{M^2 + Q^2},$$

the momentum fraction of the pomeron within the proton and the momentum fraction of the struck quark within the pomeron, respectively. The structure function is then defined by analogy to that of the total  $ep$  cross section:

$$\frac{d^3\sigma_{diff}}{d\beta dQ^2 dx_P} = \frac{2\pi\alpha^2}{\beta Q^4} (1 + (1 - y)^2) F_2^{D(3)}(\beta, Q^2, x_P),$$

where the contribution of  $F_L$  and radiative corrections are neglected and an integration over the (unmeasured)  $t$  variable is performed. The effect of neglecting  $F_L$  corresponds to a relative reduction of the cross section at small  $x_P$  (high  $W^2$ ) which is always  $< 17\%$  and therefore smaller than the typical measurement uncertainties ( $\simeq 20\%$ ).

As discussed above, a major uncertainty comes from the estimation of the non-diffractive background. This problem has been addressed in a different way in a further analysis by ZEUS [27]. In this analysis the mass spectrum,  $M^2$ , is measured as a function of  $W$  and  $Q^2$ , as shown in Figure 6 for four representative intervals, where the measured mass is reconstructed in the calorimeter and corrected for energy loss but not for detector acceptance, resulting in the turnover at large  $M^2$ . The diffractive data are observed as a low mass shoulder at low  $W$ , which becomes increasingly apparent at higher  $W$ . Also shown in the figure are the estimates of the non-diffractive background based on (a) the ARIADNE Monte Carlo (dotted histogram) and (b) a direct fit to the data, discussed below.

The probability of producing a gap is exponentially suppressed as a function of the rapidity gap, and hence as a function of  $\ln(M^2)$ , for non-diffractive interactions. The slope of this exponential is directly related to the height of the plateau distribution of multiplicity in the region of rapidity where the subtraction is made. The data can thus be fitted to functions of the form  $dN/d\ln(M^2) = D + C\exp(b \cdot \ln(M^2))$ , in the region where the detector acceptance is uniform, where  $b$ ,  $C$  and  $D$  are determined from the fits. Here,  $D$  represents a first-order estimate of the diffractive contribution which is flat in  $\ln(M^2)$ . The important parameter is  $b$ , which is determined to be  $b = 1.55 \pm 0.15$  in fits to each of the measured data intervals, compared to  $b = 1.9 \pm 0.1$  estimated from the ARIADNE Monte Carlo. The systematic uncertainty in the background reflects various changes to the fits, but in each case the measured slope is incompatible with that of the Monte Carlo. This result in itself is interesting, since the fact that ARIADNE approximately reproduces the observed forward  $E_T$  ( $\sim$  multiplicity) flow but does not reproduce the measured  $b$  slope suggests that significantly different correlations of the multiplicities are present in non-diffractive DIS compared to the Monte Carlo expectations. Also new in this analysis is that the diffractive Monte Carlo POMPYT 1.0 [28] has been tuned

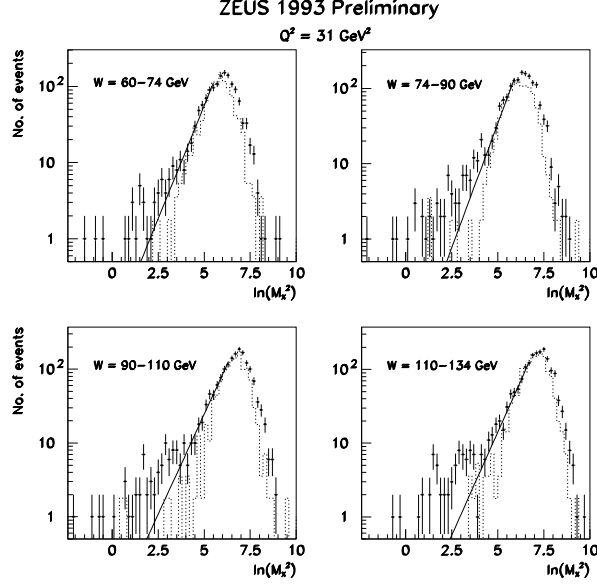


Figure 6: Preliminary ZEUS analysis of the  $\ln M^2$  distributions as a function of  $W$  at  $Q^2 = 31 \text{ GeV}^2$ . The solid lines show the extrapolation of the nondiffractive background as determined by the fits discussed in the text. The dotted histograms show the predictions for non-diffractive scattering as modelled using the ARIADNE 4.03 program.

to the observed data contribution for low mass states, allowing the high  $\beta$  region to be measured up to the kinematic limit ( $\beta \rightarrow 1$ ) and radiative corrections have been estimated in each interval ( $\lesssim 10\%$  [21]).

The virtual-photon proton cross sections measured at fixed  $M^2$  and  $W$ , measured in this analysis, can be converted to  $F_2^{D(3)}$  at fixed  $\beta$  and  $x_p$ . These results are shown in Figure 7 as the ZEUS(BGD) [27] analysis, compared to the earlier H1 [23] and ZEUS(BGMC) [24] analyses in comparable intervals of  $\beta$  and  $Q^2$  as a function of  $x_p$ . The overall cross sections in each  $\beta$  and  $Q^2$  interval are similar, however, the  $x_p$  dependences are different. As can be seen in Figure 6, the background estimates are significantly different which results in a systematic shift in the  $W$  ( $x_p$ ) dependence at fixed  $M$  ( $\beta$ ) and  $Q^2$ .

Fits of the form  $F_2^{D(3)} = b_i \cdot x_p^n$  are performed where the normalisation constants  $b_i$  are allowed to differ in each  $\beta, Q^2$  interval. The fits are motivated by the factorisable ansatz of  $F_2^{D(3)}(\beta, Q^2, x_p) = f_{IP}(x_p) \cdot F_2^{IP}(\beta, Q^2)$ , where  $f_{IP}(x_p)$  measures the flux of pomerons in the proton and  $F_2^{IP}(\beta, Q^2)$  is the probed structure of the pomeron. The exponent of  $x_p$  is identified as  $n = 1 + 2 \cdot \bar{\epsilon}$ , where  $\bar{\epsilon}$  measures the effective  $x_p$  dependence ( $\equiv W^2$  dependence at fixed  $M^2$  and  $Q^2$ ) of the cross section, integrated over  $t$ , as discussed in relation to exclusive vector meson production. In each case, the  $\chi^2/DOF$  are  $\simeq 1$  indicating that a single power law dependence on energy provides a reasonable description of the data and that effects due to factorisation breaking predicted in QCD-based calculations [29] are not yet observable. The results for  $\bar{\epsilon}$  are  $0.095 \pm 0.030 \pm 0.035$  (H1) [23],  $0.15 \pm 0.04^{+0.04}_{-0.07}$  (ZEUS(BGMC)) [24] and  $0.24 \pm 0.02^{+0.07}_{-0.05}$  (ZEUS(BGD)) [27], where the systematic errors are obtained by refitting according to a series of systematic checks outlined above. It should be noted that the ( $2\sigma$ ) systematic shift between the ZEUS(BGD) and ZEUS(BGMC) can be attributed to the method of background

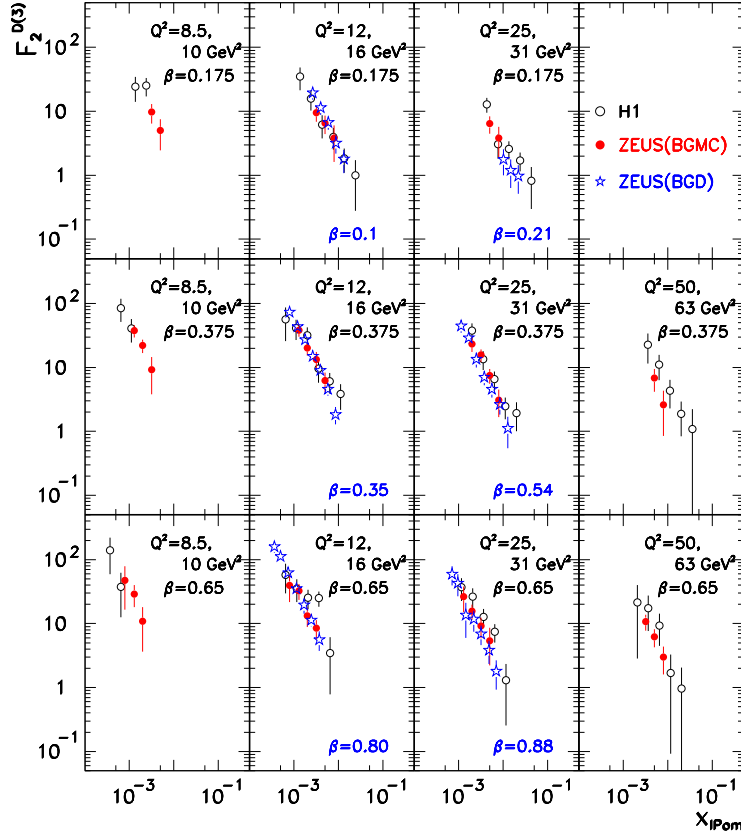


Figure 7: Comparison of the HERA data for  $F_2^{D(3)}$  as function of  $x_{IP}$  for the H1 and ZEUS(BGMC) analyses where the Monte Carlos are used to estimate the background. The upper (lower)  $Q^2$  value refers to the H1 (ZEUS) analysis. The preliminary ZEUS(BGD) where a fit to the data is used to estimate the non-diffractive background is compared at slightly different  $\beta$  values noted at the bottom of the figure.

subtraction. Whilst the H1 and ZEUS(BGMC) analyses, based on Monte Carlo background subtraction, agree within errors, the ZEUS(BGD) value is different from the H1 value at the  $3\sigma$  level.

The Donnachie-Landshoff prediction [3] is  $\bar{\epsilon} \simeq 0.05$ , after integration over an assumed  $t$  dependence and taking into account shrinkage. While comparison with the H1 value indicates that this contribution is significant, the possibility of additional contributions cannot be neglected. Taking the ZEUS(BGD) value, this measurement is incompatible with the predicted soft pomeron behaviour at the  $4\sigma$  level. Estimates of the effect of  $\sigma_L$  made by assuming  $\sigma_L = (Q^2/M^2)\sigma_T$  rather than  $\sigma_L = 0$  result in  $\bar{\epsilon}$  increasing from 0.24 to 0.29.

The values can also be compared with  $\bar{\epsilon} \simeq 0.2$  obtained from the exclusive photoproduction of  $J/\psi$  mesons and the electroproduction data or with  $\epsilon \simeq 0.2$  to 0.25 obtained from the dependence of the total cross sections in the measured  $Q^2$  range [18]. In the model of Buchmüller and Hebecker [30], the effective exchange is dominated by one of the two gluons. In terms of  $\epsilon$ , where the optical theorem is no longer relevant, the diffractive cross section would therefore rise with an effective power which is halved to  $\epsilon \simeq 0.1$  to 0.125. The measured values are within the range of these estimates.

The overall cross sections in each  $\beta$ ,  $Q^2$  interval are similar and one can integrate over the measured  $x_p$  dependence in order to determine  $\tilde{F}_2^D(\beta, Q^2)$ , a quantity which measures the internal structure of the pomeron up to an arbitrary integration constant. Presented in this integrated form, the data agree on the general features of the internal structure. In Figure 8 the H1 data are compared to preliminary QCD fits [31]. The general conclusions from the  $\beta$  dependence are that the pomeron has a predominantly hard structure, typically characterised by a symmetric  $\beta(1-\beta)$  dependence, but also containing an additional, significant contribution at low  $\beta$  which has been fitted in the ZEUS analysis [24]. The virtual photon only couples directly to quarks, but the overall cross section can give indications only of the relative proportion of quarks and gluons within the pomeron, since the flux normalisation is somewhat arbitrary [24]. The  $Q^2$  behaviour is broadly scaling, consistent with a partonic structure of the pomeron. Probing more deeply, however, a characteristic logarithmic rise of  $\tilde{F}_2^D$  is observed in all  $\beta$  intervals. Most significantly, at large  $\beta$  a predominantly quark-like object would radiate gluons resulting in negative scaling violations as in the case of the large- $x$  ( $\gtrsim 0.15$ ) behaviour of the proton. The question of whether the pomeron is predominantly quarks or gluons, corresponding to a “quarkball” or a “gluomeron” [32], has been tested quantitatively by H1 using QCD fits to  $\tilde{F}_2^D$  [31]. A flavour singlet quark density input of the form  $zq(z) = A_q \cdot z^{B_q}(1-z)^{C_q}$ , where  $z$  is the momentum fraction carried by the quark, yields a numerically acceptable  $\chi^2$ . The characteristic  $Q^2$  behaviour, however, is not reproduced. Adding a gluon contribution of similar form gives an excellent description of the data. The fit shown uses  $B_q = 0.35$ ,  $C_q = 0.35$ ,  $B_g = 8$ ,  $C_g = 0.3$ . In general, the fits tend to favour inputs where the gluon carries a significant fraction,  $\sim 70$  to  $90\%$ , of the pomeron’s momentum.

## 2.3 Jet structure

The question of the constituent content of the pomeron can also be addressed via measurements of diffractively produced jets in the photoproduction data [33]. Jets are reconstructed at large  $W$  ( $130 < W < 270$  GeV) using the cone algorithm with cone radius 1 and  $E_T^{jet} > 8$  GeV. The diffractive contribution is identified as a tail in the  $\eta_{max}$  distribution of these events above

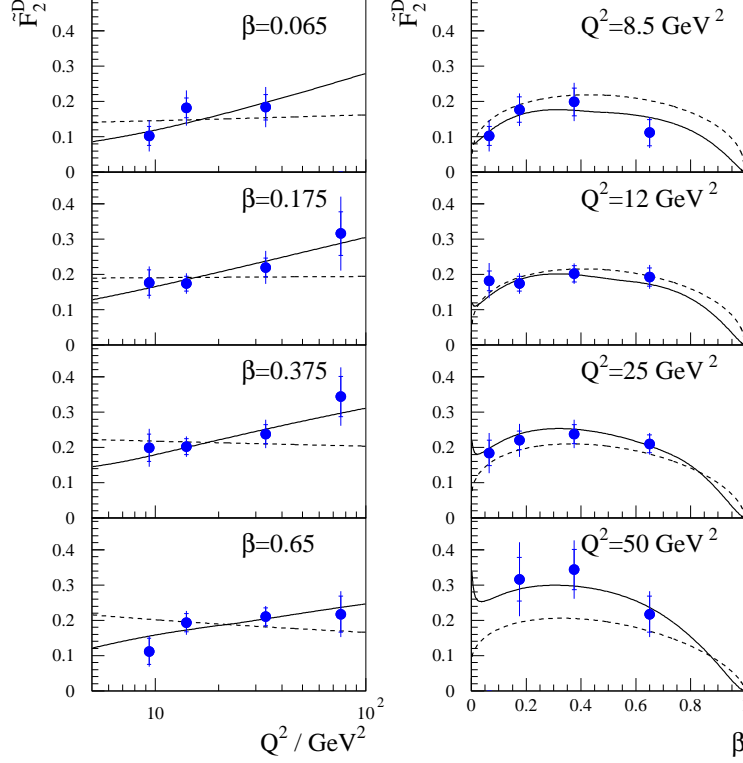


Figure 8: H1 data on  $\tilde{F}_2^D(\beta, Q^2)$  as a function of  $Q^2$  ( $\beta$ ) at fixed  $\beta$  ( $Q^2$ ). The data are compared to preliminary leading-order QCD fits where: (a) only quarks are considered at the starting scale,  $Q_0^2 = 4 \text{ GeV}^2$ , indicated by the dashed line ( $\chi^2/DOF = 13/12$ , 37% CL); (b) gluons also contribute at the starting scale, resulting in a fit where gluons carry  $\sim 90\%$  of the momentum, indicated by the full line ( $\chi^2/DOF = 4/9$ , 91% CL).

the PYTHIA 5.7 [34] Monte Carlo expectation. In Figure 9(a) the measured cross section is compared to various model predictions as a function of the jet rapidity. Comparison with the non-diffractive contribution estimated from PYTHIA indicates a significant excess at lower values of  $\eta^{jet}$ . Here, standard photon and proton parton distributions are adopted and the overall scale, which agrees with the non-diffractive data normalisation, is set by  $E_T^{jet}$ . Also shown are the predicted diffractive cross sections from POMPYT using a hard ( $z(1-z)$ ) quark, hard gluon or soft  $((1-z)^5)$  gluon where a Donnachie-Landshoff flux factor is adopted and the momentum sum rule is assumed to be satisfied in each case. Sampling low-energy (soft) gluons corresponds to a small cross section and can be discounted, whereas high-energy (hard) gluons and/or quarks can account for the cross section by changing the relative weights of each contribution. The  $x_\gamma$  distribution for these events, where  $x_\gamma$  is the reconstructed momentum fraction of the interacting photon, is peaked around 1, indicating that at these  $E_T^{jet}$  values a significant fraction of events is due to direct processes where the whole photon probes the pomeron constituents.

We now have two sets of data, the DIS data [24] probing the pomeron structure at a scale  $Q$  and the jet data probing at a scale of  $E_T^{jet}$ . Each probes the large  $z$  structure of the pomeron with the jet and DIS data, predominantly sampling the (hard) gluon and quark distributions,

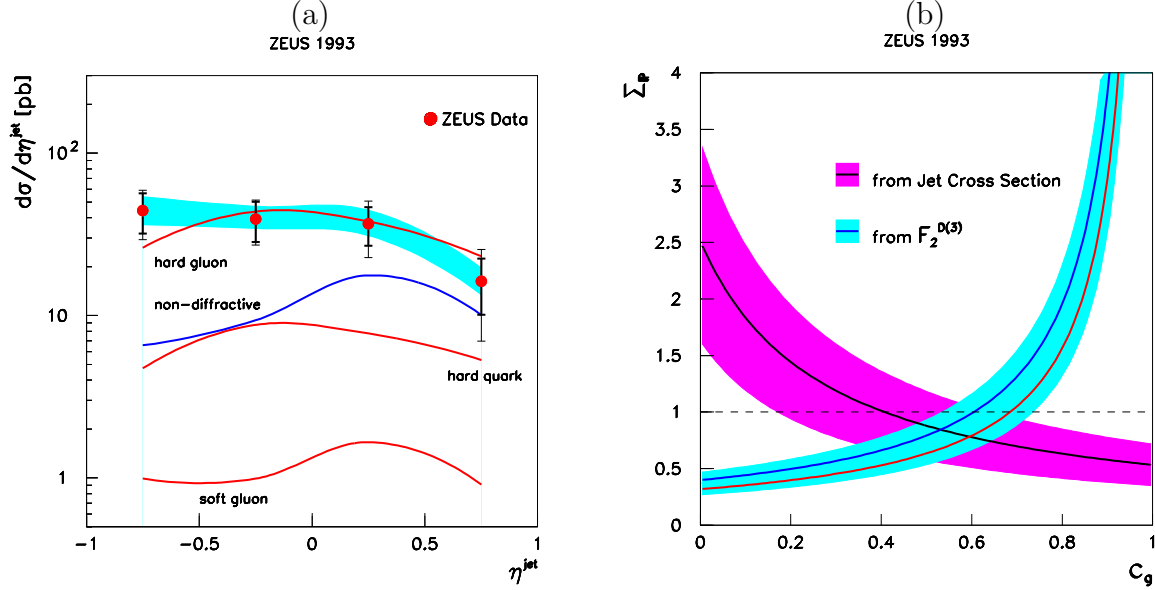


Figure 9: (a) Jet cross section as a function of jet rapidity for events with  $\eta_{max} < 1.8$ . (b) Momentum sum rule assuming a Donnachie-Landshoff flux,  $\Sigma_P$ , versus the momentum fraction carried by the gluons in the pomeron,  $c_g$ . The dark (light) error bands correspond to statistical errors on the fits to the jet (DIS) data discussed in the text.

respectively. In Figure 9(b) the preferred momentum fraction carried by the (hard) gluon,  $c_g$ , is indicated by the overlapping region of the jet (dark band) and DIS (light band) fits to the data. Considering the systematics due to the non-diffractive background, modelled using the Monte Carlo models, a range of values consistent with  $c_g \sim 0.55 \pm 0.25$  can be estimated. The result depends on the assumption that the cross sections for both sets of data factorise with a universal flux, characterised by the same value of  $\bar{e}$  in this  $W$  range, but does not assume the momentum sum rule.

So far we have only considered the case of small- $t$  diffraction with respect to the outgoing proton. Further insight into the diffractive exchange process can be obtained by measurements of the rapidity gap between jets. Here, a class of events is observed with little hadronic activity between the jets [35]. The jets have  $E_T^{jet} > 6$  GeV and are separated by a pseudorapidity interval ( $\Delta\eta$ ) of up to 4 units. The scale of the momentum transfer,  $t$ , is not precisely defined but is of order  $(E_T^{jet})^2$ . A gap is defined as the absence of particles with transverse energy greater than 300 MeV between the jets. The fraction of events containing a gap is then measured as a function of  $\Delta\eta$ , as shown in Figure 10. The fit indicates the sum of an exponential behaviour, as expected for non-diffractive processes and discussed in relation to the diffractive DIS data, and a flat distribution expected for diffractive processes. At values of  $\Delta\eta \gtrsim 3$ , an excess is seen with a constant fraction over the expectation for non-diffractive exchange at  $\simeq 0.07 \pm 0.03$ . This can be interpreted as evidence for large- $t$  diffractive scattering. In fact, secondary interactions of the photon and proton remnant jets could fill in the gap and therefore the underlying process could play a more significant rôle. The size of this fraction is relatively large when compared to a similar analysis by D0 and CDF where a constant fraction at  $\simeq 0.01$  is observed [36, 37]. The relative probability may differ due to the higher  $W$  values of the Tevatron compared to

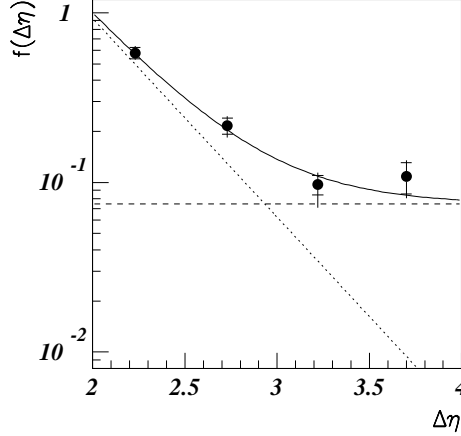


Figure 10: Gap-fraction,  $f(\Delta\eta)$ , as a function of the rapidity gap between the two jets compared with the result of a fit to an exponential plus a constant.

HERA or, perhaps, due to differences in the underlying  $\gamma p$  and  $p\bar{p}$  interactions.

## 2.4 Leading proton spectrometer measurements

The advent of the leading proton spectrometers (LPS) at HERA is especially important in these diffractive measurements, since internal cross checks of the measurements as a function of  $t$ ,  $M^2$ ,  $W^2$  and  $Q^2$  can ultimately be performed and underlying assumptions can be questioned experimentally. Only in these measurements can we positively identify the diffracted proton and hence substantially reduce uncertainties on the non-diffractive and double dissociation backgrounds. However, new uncertainties are introduced due to the need for precise understanding of the beam optics and relative alignment of the detectors. Reduced statistical precision also results due to the geometrical acceptance of the detectors ( $\simeq 6\%$ ). In figure 11(a), various observed distributions are shown for 240 events selected from the DIS data, with  $Q^2 \gtrsim 4 \text{ GeV}^2$ . The momentum distribution clearly indicates a significant diffractive peak at  $E_p = 820 \text{ GeV}$  above the non-diffractive background and the observed  $M$  and  $W$  distributions are well described by the NZ Monte Carlo [38]. The distribution of  $\beta$  versus  $x_p$  indicates a significant fraction of events at small  $\beta \lesssim 0.1$  which are difficult to access using the experimental techniques described earlier. The measurements are currently being analysed, but a preliminary result on the  $t$ -dependence is shown in Figure 11(b), measured in a relatively high observed mass interval,  $\langle M \rangle = 9 \text{ GeV}$ , at relatively low  $Q^2$ . The slope can be characterised by a single exponential fit with  $b = 7.52 \pm 0.95^{+0.65}_{-0.82}$ . This is somewhat high compared to the value of  $b \simeq 4.5$  expected for a predominantly hard pomeron but lies within the range of expectations of  $4 \lesssim b \lesssim 10$ . However, before drawing conclusions, we should perhaps wait for further results on the general dependences measured in the LPS.

## 3 Conclusions

The soft pomeron no longer describes *all* diffractive data measured at HERA. As the photon virtuality and/or the vector meson mass increases a new dependence on  $W^2$  emerges. As we

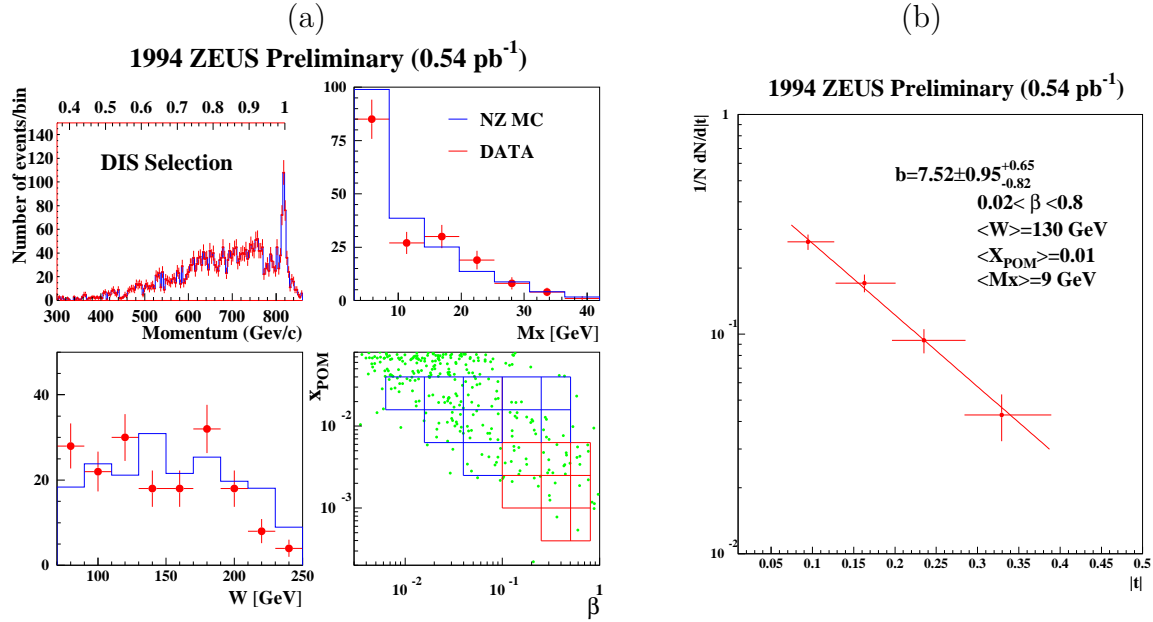


Figure 11: (a) Observed momentum,  $M$ ,  $W$  and  $\beta$  versus  $x_p$  distributions in the LPS. The observed  $M$  and  $W$  distributions are compared to the NZ Monte Carlo predictions. (b) Corrected  $t$  distribution in the quoted range.

investigate the pomeron more closely, a new type of dynamical pomeron may begin to play a rôle: a dynamical pomeron whose structure is being measured in DIS. These data are consistent with a partonic description of the exchanged object which may be described by pQCD. The experimental work focuses on extending the lever arms and increasing the precision in  $t$ ,  $M^2$ ,  $W^2$  and  $Q^2$  in order to explore this new structure. Before more precise tests can be made, further theoretical and experimental input is required to reduce the uncertainties due to non-diffractive backgrounds and proton dissociation as well as the treatment of  $F_L$  and radiative corrections.

## Acknowledgements

The results presented in this talk are a summary of significant developments in the study of diffraction at HERA during the last year. The financial support of the DESY Directorate and PPARC allowed me to participate in this research, whilst based at DESY, for which I am very grateful. It is a pleasure to thank Halina Abramowicz, Ela Barberis, Nick Brook, Allen Caldwell, John Dainton, Robin Devenish, Thomas Doeker, Robert Klanner, Henri Kowalski, Aharon Levy, Julian Phillips, Jeff Rahn, Laurel Sinclair, Ian Skillicorn, Ken Smith, Juan Terron, Jim Whitmore and Günter Wolf for their encouragement, enthusiasm, help and advice. Finally, thanks to Mike Whalley for his organisation at the workshop and for keeping me to time in these written proceedings.

## References



- [1] G. Ingelman, J. Phys. G19 (1993) 1633.
- [2] K. Goulianos, Phys. Rep. 101 (1983) 169; Nucl. Phys. B (Proc. Suppl.) 12 (1990) 110.
- [3] A. Donnachie and P.V. Landshoff, Nucl. Phys. B244 (1984) 322; A. Donnachie, these proceedings.
- [4] CDF Collab., F. Abe et al., Phys. Rev. D50 (1994) 5550.
- [5] H1 Collab., S. Aid et al., EPS-0473.
- [6] ZEUS Collab., M. Derrick et al., DESY 95-143.
- [7] H1 Collab., S. Aid et al., EPS-0490.
- [8] ZEUS Collab., M. Derrick et al., Phys. Lett. B356 (1995) 601.
- [9] ZEUS Collab., M. Derrick et al., EPS-0389.
- [10] ZEUS Collab., M. Derrick et al., EPS-0397.
- [11] H1 Collab., S. Aid et al., EPS-0468.
- [12] ZEUS Collab., M. Derrick et al., EPS-0386.
- [13] H1 Collab., S. Aid et al., EPS-0469.
- [14] H. Holtmann et al., HEP-PH-9503441.
- [15] CDF Collab., F. Abe et al., Phys. Rev. D50 (1994) 5535.
- [16] D. Aston et al., Nucl. Phys. B209 (1982) 56.
- [17] G.A. Schuler and T. Sjöstrand, Nucl. Phys. B407 (1993) 539.
- [18] A. Levy, DESY 95-204.
- [19] M. Ryskin et al., these proceedings.
- [20] M. Glück, E. Reya and A. Vogt, Phys. Lett. B306 (1993) 391.
- [21] N. Wulff, University of Hamburg thesis (1994), unpublished.
- [22] C. Berger, Proceedings of the Beijing Conference, August 1995.
- [23] H1 Collab., T. Ahmed et al., Phys. Lett. B348 (1995) 681; J. Dainton, DESY 95-228.
- [24] ZEUS Collab., M. Derrick et al., Z. Phys. C68 (1995) 569.
- [25] G. Ingelman and K. Jansen-Prytz, Z. Phys. C58 (1993) 285.
- [26] L. Lönnblad, Comp. Phys. Comm. 71 (1992) 15.

- [27] ZEUS Collab., M. Derrick et al., Contribution to the Beijing Conference, August 1995.
- [28] P. Bruni and G. Ingelman, DESY 93-187; Proceedings of the Europhysics Conference on HEP, Marseille 1993, 595.
- [29] N.N. Nikolaev and B.G. Zakharov, Z. Phys. C53 (1992) 331; M. Genovese, N.N. Nikolaev and B.G. Zakharov, KFA-IKP(Th)-1994-37 and CERN-TH.13/95.
- [30] W. Buchmüller and A. Hebecker, DESY 95-077.
- [31] H1 Collab., S. Aid et al., EPS-0491; J.P. Phillips, Proceedings of the Paris Conference, April 1995.
- [32] F. Close and J. Forshaw, HEP-PH-9509251.
- [33] ZEUS Collab., M. Derrick et al., Phys. Lett. B356 (1995) 129.
- [34] H.-U. Bengtsson and T. Sjöstrand, Comp. Phys. Comm. 46 (1987) 43; T. Sjöstrand, CERN-TH.6488/92.
- [35] ZEUS Collab., M. Derrick et al., DESY 95-194.
- [36] D0 Collab., S. Abachi et al., Phys. Rev. Lett. 72 (1994) 2332; D0 Collab., S. Abachi et al., FERMILAB-PUB-95-302-E (1995).
- [37] CDF Collab., F. Abe, et al., Phys. Rev. Lett. 74 (1995) 855.
- [38] A. Solano, Ph.D. Thesis, University of Torino 1993 (unpublished); A. Solano, Nucl. Phys. B (Proc. Suppl.) 25 (1992) 274.